WILEY-VCH

Polymer-assisted metallization of mammalian cells

*Wenshuo Wang, Qi Gan, Yuqi Zhang, Xi Lu, Huixin Wang, Yaokang Zhang, Hong Hu, Lina Chen, Lianxin Shi, Shutao Wang, Zijian Zheng**

Dr. W. Wang, Dr. Q. Gan, Dr. Y. Zhang, Dr. X. Lu, H. Wang, Dr. Y. Zhang, Dr. H. Hu, Dr. L. Chen, Prof. Z. Zheng
Laboratory for Advanced Interfacial Materials and Devices
Institute of Textiles and Clothing
The Hong Kong Polytechnic University
Hong Kong SAR, China
E-mail: tczzheng@polyu.edu.hk

Dr. L. Shi, Prof. S. Wang
CAS Key Laboratory of Bio-inspired Materials and Interfacial Science
CAS Center for Excellence in Nanoscience
Technical Institute of Physics and Chemistry, Chinese Academy of Sciences
Beijing, 100190, P. R. China

Prof. S. Wang
School of Future Technology
University of Chinese Academy of Sciences
Beijing, 100049, P. R. China

Keywords: cell metallization, polymer-assisted metal deposition, biotemplating, biocomposites, nanomaterials

Abstract

Developing biotemplating techniques to translate microorganisms and cultured mammalian cells into metallic biocomposites is of great interest in biosensors, electronics, and energy. The metallization of virus and microbial cells has been successfully demonstrated via genetic engineering strategy or electroless deposition. However, mammalian cells are difficult to transform into metallic biocomposites because of the complicated genes and the delicate morphological features. Herein, we report "polymer-assisted cell metallization" (PACM) as a general method for the transformation of mammalian cells into metallic biocomposites. PACM includes a first step of in-situ polymerization of functional polymer on the surface and in the interior of the mammalian cells, and a subsequent electroless deposition of metal to convert the polymer-functionalized cells into metallic biocomposites, which retain the micro- and nano-structures of the mammalian cells. This new biotemplating method is compatible with different cell types and metals to yield a wide variety of metallic biocomposites with controlled structures and properties.

Main text

Biotemplating technologies translate biological materials in nature into synthetic materials with special structures and properties that are difficult to fabricate through artificial synthesis.[1] In the past two decades, biotemplating strategies for engineering metallic biocomposites[2-6] have received considerable attention because of the marked electrical, magnetic, and chemical properties associated with these unique materials and their broad application potentials in the fields of biosensor, microrobotics, electronics, catalysis, and energy.[7-11]

Generally, the metallization of biotemplates can be realized in two strategies including 1) the nucleation and growth of metal with metallophilic peptides produced through gene engineering,[3,6] and 2) direct electroless deposition (ELD) of metal on biotemplates.[11,12] The former makes use of metallophilic peptides, which are expressed on genetically engineered microbes, to anchor metal salt precursors for subsequent metallization. Nevertheless, this strategy is complicated and can only be applied to biotemplates with simple genes such as viruses and microbial cells. In contrast, the second strategy is much easier to achieve by direct ELD on different kinds of biotemplates. The challenge of this method, however, is the difficulty in retaining the complex and soft structures of the biotemplates during the metal plating. Therefore, the ELD strategy is only applicable to biotemplates with simple or rigid structures including oligonucleotides, virus, cell-wall-encased microorganisms (e.g., bacteria and algae), and macroscopic biological units. [2,5,11-15]

Compared with viruses and cell-wall-encased microorganisms, mammalian cells possess much more special features, including hierarchical structures, tunable morphologies, and the feasibility of forming large-area assemblies such as cell sheets.[16] These features are attractive as biotemplates for fabricating anisotropic materials and assemblies with advanced functions.[17-22] For example, an elegant silicification approach has been developed to fabricate

silica-based replicas of mammalian cells and biological tissues.[17,23] Moreover, carbonized replicas or metal-nanoparticles-decorated silica replicas of mammalian cells can be derived by combining the silicification method with post-treatment such as carbonization or infiltration and reduction of metal ions.[17,18] However, the metallization of mammalian cells has not been reported up to now. From a chemical perspective, mammalian cells lack metallophilic components to control the metal binding or growth, so that it is difficult to retain the complex hierarchical biostructures during metal deposition. Biologically, mammalian cells possess complicated genes, making the gene-engineering approach infeasible.

Herein, we report a general and versatile method named polymer-assisted cell metallization (PACM), which can precisely control the metallization of mammalian cells and preserve the deliciated surface structures in the metallic biocomposites. PACM makes use of metallophilic polymers, which are polymerized in situ on the surfaces and in the body of targeted mammalian cells, as binding sites for subsequent ELD of metal. By controlling the polymerization and metallization conditions, PACM allows the fabrication of metallic biocomposites with different cell types such as C2C12 cells, HeLa cells, and HCT8 cells, various metal species such as Cu, Ni, Ag, and bimetals, and controllable architectures such as wrinkled and jellyfish-like structures. Apart from the structural features inherited from the cell templates, the metallic biocomposites also show metal properties such as conductive and magnetic properties. We demonstrate the applications of cell-templated metallic biocomposites for the construction of superaerophobic electrodes and magnetic biohybrids.

As shown in **Figure 1**A, the PACM process is comprised of on-cell polymerization, ion exchange, and electroless deposition. The on-cell polymerization allows for in situ grafting of metallophilic polymer chains on the surface and in the body of the mammalian cells, while the

subsequent ion exchange and ELD convert the polymer-functionalized cells into metallic biocomposites with a good preservation of the cell morphology.

As a proof-of-concept, murine myoblasts (C2C12 cells) were firstly fixed and treated with triton x-100 to enhance the permeability of the cell membrane. The pretreated cells were then incubated with acrylic acid N-hydroxysuccinimide ester (NHS-AA) to immobilize vinyl groups on the surface and in the interior of the cells, where NHS-AA molecules react with the amine groups of cell proteins. After sufficient rinsing, the vinyl-immobilized C2C12 cells were immersed into the polymerization solution containing initiator ammonium persulfate (APS), promoter tetramethylethylenediamine (TEMED), and monomer 2-(methacryloyloxy) ethyltrimethylammonium chloride (METAC) to carry out the free radical polymerization at 37 °C. Poly(methacryloyloxy) ethyltrimethylammonium chloride (PMETAC) synthesized in the polymerization reaction were covalently immobilized on and inside the cells by the vinyl groups. The PMETAC-immobilized C2C12 cells were then immersed into an $(NH_4)_2PdCl_4$ solution, in which the $PdCl_4^{2-}$ ions exchanged with the Cl^- because of their higher affinity to the quaternary ammonium groups of METAC. The $PdCl_4^{2-}$ ions are known as a highly active species to promote electroless deposition. Finally, cells loaded with $PdCl_4^{2-}$ ions were immersed in the plating bath of Cu to carry out ELD, and the cells were transformed into Cu-based biocomposites with a good preservation of the micro- and nano-structures of the C2C12 cells (Figure 1B).

Elemental mapping at different stages of the chemical reactions evidenced the transformation of materials (Figure 1C). The elemental mapping showed little difference before and after polymerization of the C2C12 cells (i and ii), because both the PMETAC and cells are rich in C, N, and O. Strong Pd and Cl peaks were observed after the ion exchange with $PdCl_4^{2-}$ (iii), indicating a success and large amount of immobilization of $PdCl_4^{2-}$ ions. After the metallization

step, the Pd and Cl peaks disappeared and the Cu peak raised (iv), indicating that Cu was grown from the surface of Pd seeds in the ELD process.

PMETAC plays a critical role in enabling the metal deposition and the anchoring of the metal layer on the cell surface and inside the cells. To demonstrate the successful immobilization of PMETAC, we incubated C2C12 cells, which were reacted at different polymerization time, with negatively charged fluorescent probes 1,3,6,8-pyrenetetrasulfonic acid tetrasodium salt (4-PSA). The anionic 4-PSA has a strong binding affinity to the cationic PMETAC due to the electrostatic interactions between the counter ions (**Figure 2**A,B). Longer polymer chains shall adsorb more 4-PSA dyes, thus forming more excimers and stronger fluorescence.[24,25]

Fluorescent microscopy study showed distinct fluorescence signals of the stained cells with polymerization time longer than 5 min (Figure 2A). The values of fluorescent intensity of the cell samples were plotted in Figure 2B. These results correspond to the three classical polymerization stages including initiation, propagation, and termination. We could infer from the results that the first 5-min incubation was attributed to the initiation step of the free radical polymerization because no obvious fluorescent signal was detected. Chain propagation occurred in between 5 min and 30 min. At this stage, a longer polymerization time led to higher intensity of the fluorescent signal of the treated cells, revealing that more dyes were adsorbed because longer polymer chains were synthesized. After polymerization for 30 min, the fluorescent intensity reached a plateau, indicating the cease of chain growth due to termination. Furthermore, the confocal images (Figure 2C and Figure S1, Supporting Information) confirmed that the polymerization occurred both on the surface of and inside the cells. The polymerization study confirms that monomers and initiators not only reacted on the surface of the cells, but also penetrated through the cell membrane and conducted polymerization inside the cells to form long chains.

Importantly, the existence of the polymer interlayer is vital to the success of cell metallization. We conducted metallization of cells with different polymerization time of 0, 5, 15, 30, 45, and 60 min, followed by the standard ion exchange and ELD processes. The immobilization of $PdCl_4^{2-}$ was enhanced at increased polymerization times (Figure 2D). After the ELD process, cells exhibited different metallization performances related to the polymerization times (Figure 2E and Figure S2, Supporting Information). Without polymerization, the soft cells collapsed because of the evaporation of water during the sample preparation. In contrast, with polymerization time longer than 30 min, metallization of cells was successfully realized. The microscale spherical structure and the ruffled membrane, as well as the nanoscale villi of the C2C12 cells, were well preserved in the metallized cells, all of which were uniformly coated with Cu. The diameters of the villi on the cell surface increased from an average of about 80 nm to 180 nm after metallization across the three-dimensional cell body (Figure 2F–H). With a short polymerization time, i.e., 5~15 min, metallization also occurred. However, the cells partially collapsed and the nanostructures on the cell surface could not be fully preserved.

It should be noted that the metallization firstly occurred at the surfaces of the cells, at which a metallic shell was formed (Figure 2I). After further metal deposition for about 20 min, the interior space of the cells was fully metallized (Figure 2J and Figure S3, Supporting Information). The good preservation of micro- and nano-structures is attributed to the rapid reinforcement of cells at the early stage of the metal coating, especially with a high concentration of polymer chains. We measured the elastic modulus of cells before and after metallization by atom force microscope (AFM) and nanoindenter, respectively. The AFM-derived force-displacement curve of non-metallized cells showed a slow increase of force as a function of displacement depth (Figure S4A, Supporting Information), which is a typical response of soft materials. The elastic modulus of C2C12 cells before metallization was about

70 kPa (Figure 2K). In contrast, the force experienced on the metallized cells elevated rapidly (Figure S4B, Supporting Information), which indicates a much stiffer substrate. The mechanical characterization of Cu-metallized C2C12 cells was carried out by a nanoindenter system, which is more suitable for probing stiff materials.[26] The calculated elastic modulus of metallized cells increased dramatically to 16 GPa after metallization of 5 min and reached about 30 GPa after fully metallized (Figure 2K). The deposited metal strongly adhered to cells by the polymer chains and reinforced the three-dimensional cell body and cell surfaces. The enhanced stiffness overcame the structural collapse caused by the capillary force in the drying process. As such, the original soft micro- and nano-structures of the cell can be well retained by PACM.

Importantly, PACM is versatile to synthesize cell-based metallic biocomposites with a combination of a wide variety of biotemplates, metals, and tunable architectures. As a proof of concept, we tested the PACM technique with different mammalian cell templates including C2C12, HeLa, and HCT8 cells with different states (spreading on substrate or suspended in solution). As shown in **Figure 3**A, the Cu-metallized biocomposites displayed morphological characteristics of their corresponding biotemplates. It is worth noting that the morphology of mammalian cells can be easily tuned and then transformed into metallic biocomposites with more specific structures,[18] making it possible to fabricate metallic biocomposites with different structures by using the same cell line. For example, we pre-treated living HCT8 cells by adding polyethylene glycol (PEG) in the cell culture medium. PEG made the culture medium hypertonic and led to cell shrinkage. We performed PACM using the shrunk cells as templates, where wrinkled metallic biocomposites with hierarchical structures were formed (Figure 3B). In addition to mammalian cells, the PACM strategy could be easily adopted to many other biological templates such as extracellular vesicles, yeasts, and pollen grains (Figure S5, Supporting Information), further demonstrating that the polymer-assisted metallization method is a powerful and general biotemplating technique.

Apart from Cu discussed above, PACM can synthesize biocomposites with other metals. We synthesized Ni-based and Ag-based biocomposites with PACM using HeLa and HCT8 cells, respectively. Again, all the fine structures of the cell templates were well preserved (Figure 3C and Figures S6,S7, Supporting Information). In addition, we synthesized bimetallic biocomposites with the combination of PACM and galvanic displacement reaction.[27-29] In brief, HCT8 cells metallized with Cu were immersed in a $HAuCl_4$ solution, where galvanic displacement reaction took place to produce Cu/Au bimetal biocomposites. The bimetallic biocomposites exhibit a similar morphology to the Cu-only biocomposite and the original HCT8 cell at a displacement time under 5 min (Figure 3D and Figure S8, Supporting Information). With an additional sacrificial layer of polymethyl methacrylate (PMMA), we further prepared jellyfish-like Janus biocomposites, in which the inner side of the biocomposites was decorated with Pt and the outer surface was coated with Cu (Figure 3E and Figure S9, Supporting Information). In the solution containing H_2O_2, Pt could catalyze the generation of O_2 bubbles, thus producing asymmetric force to propel the cell-templated Janus microparticle (Figure S9 and Movie S1, Supporting Information).

These metallic biocomposites inherit a combination of the morphological features of the original mammalian cell and the intrinsic properties of the metal, and hence result in unique features do not afford by other biocomposites. We demonstrate here two applications of the mammalian-cell-templated biocomposites, including the construction of the electrochemical-active and superwetting electrode for efficient hydrogen evolution reaction (HER), and smart capture and manipulation of living cells.

First, our proposed metallic biocomposites are suitable for constructing superwetting electrodes to improve the performance of gas-involving electrocatalysis.[30-35] The electrical conductivity

of a single Cu-metallized C2C12 cell is about 3.4 Ω, which was measured by a cantilever probe mounted on an AFM platform (Figure 4A). We then fabricated a highly conductive electrode (0.28 Ω sq^{-1}) made of a continuous sheet of Cu-metallized C2C12 cells and denoted it as C2C12-Cu electrode. The C2C12-Cu electrode exhibited superaerophobicity with an underwater bubble contact angle of 156.9 ± 3.8° (Figure 4B and Figure S10, Supporting Information), which is an advantage in the HER. In the process of HER, H_2 bubbles were generated on and then escaped easily from the surface of the C2C12-Cu electrode (Figure 4C), because the hierarchical superaerophobic surface afforded a discontinuous three-phase (solid−liquid−gas) contact line, and thus dramatically reduced the adhesion of H_2 bubbles.[33] The fast removal of small bubbles could maximize the working surface area of the electrode and benefit the energy efficiency of the catalytic reaction, which can be verified by the rapid increase in current density upon the increase of the potential. In contrast, gas bubbles adhered to the surface of a flat Cu electrode, and did not escape until their sizes grew large enough to provide an adequate buoyancy overtaking the adhesion force (Figure 4C). These tightly adhered and large-sized bubbles severely blocked the diffusion of electrolytes and hence hindered the HER at those areas. Under an applied potential of -0.7 V, the current density of the C2C12-Cu electrode reached 17.3 mA cm^{-2}, which is more than 10 folds of that of the flat Cu electrode (1.6 mA cm^{-2}) (Figure 4D).

Second, we demonstrated the efficient adhesion and manipulation of living mammalian cells using cell-templated ferromagnetic biocomposites. The prepared C2C12-Ni biocomposites showed a typical ferromagnetic property, making such biocomposites easily manipulated by an external magnetic field (Figure 5A). It is known that specific chemical and/or biological modification of a surface is normally needed to enhance the adhesion with target cells. In our case, we realized an enhanced adhesion by simply using the structural similarity between biocomposites and living cells. Without further specific modification, C2C12-Ni biocomposites

could adhere intimately onto target cells through strong topographic interaction, benefiting from the well-preserved topography and morphology of the cell templates after PACM (Figure 5B). The strong structural connection between the ferromagnetic biocomposites and living cells facilitated the assembly of stable biohybrids with various formats (Figure 5C), which could be easily controlled under a magnetic field. As such, we demonstrated the use of these assembled biohybrids as magnetic-responsive microrobots to target and manipulate living cells (Figure 5D and Movie S2, Supporting Information).

To further quantify the enhancement of adhesion of metallic biocomposites with different cell types, we incubated C2C12-Ni, HTC8-Ni, metallic chrysanthemum pollen grains (pollen-Ni), and smooth polystyrene (PS) microparticles, respectively, with living C2C12 cells, living HTC8 cells, and fixed cells (fixed C2C12 and fixed HTC8). We then counted the numbers of those microparticles adhered to cells and the statistical results are displayed in Figure 5E. We found that the metallic biocomposites based on mammalian cells, i.e., C2C12-Ni and HTC8-Ni, showed significantly improved adhesion to living cells. For example, the number of C2C12-Ni adhered to living C2C12 cells was significantly greater than pollen-Ni (c.a. 2 folds) and PS microparticles (c.a. 11 folds). This result further supports the importance of the perseveration of nanostructures through the PACM process, where living cells adhere much more easily to nanostructured biocomposites (C2C12-Ni and HTC8-Ni) than microstructured biocomposites (pollen-Ni), and are difficult to adhere to the smooth surface (PS). We also found that C2C12-Ni and HTC8-Ni showed similar adhesion to the two living cells. This can be explained by the fact that both biocomposites possessed similar nanoscale metallic villi structures at the subcellular level. It is known that in the process of adhesion, living mammalian cells will interact with the extracellular environment with their soft surface nanostructures and adapt to different shapes. The results of the control experiments, where metallic biocomposites hardly

adhered to any fixed mammalian cells, also demonstrated the importance of soft nanostructures of living cells in the adhesion process.

In summary, we report the first polymer-assisted cell metallization strategy for transforming mammalian cells into functional metallic biocomposites with precise maintenance of original cell structures. Layer-by-layer assembly of polymer chains and in situ polymerization techniques have received increasing attention in recent years to direct cell encapsulation,[36-39] to control cell behaviors,[40,41] to implement cell labelling and intracellular nanomaterial synthesis,[42] to achieve expanded cell imaging,[43,44] and to realize cell-specific stimulation.[45] On the other hand, surface-grafted polymer chains are known to be used as interfacial layers for deposition of metallic species on many non-conductive fibers, textiles, and films.[46-50] Given the wide use of various polymers for both cell engineering and metal deposition, here the polymer is exploited to bridge mammalian cells and metals, and thus to achieve controllable transformation of cells into metallic biocomposites.

PACM is a simple biotemplating synthesis method, in which the polymer grafting and metal deposition can be readily realized in solution without relying on any expensive devices. In PACM, the polymer interlayer is the key element to achieve the precise control of metal deposition. The polymer chains immobilized on the surface and in the interior of mammalian cells provide ample binding sites for ionic moieties that are essential to carry out the metal deposition, and ensure sufficient intracellular metallization and conformal surface coating of metal on arbitrary and nanostructured mammalian cells. PACM method is general and versatile. PACM enables the facile synthesis of a variety of biomorphic materials such as suspended and adhered metallic biocomposites using mammalian cells as biotemplates. In addition, as a general technique, the PACM is compatible with several different electroless metal plating systems. The integration of mammalian cells and metals can produce advanced metallic

biocomposites with a wide range of applications. For example, the cell-templated Cu electrode with superaerophobic property is beneficial to high performance in hydrogen evolution reaction. The magnetic biocomposites with cell structures are also very promising for bio-interfacing with living cells to form stable magnetic biohybrids and for cell manipulation. Therefore, PACM provides a very powerful technique that allows the preparation of metallic biocomposites with tunable size, shape, structure, and composition of metal, which provide unique and important properties for applications in biological, optical, electronic, and energy-related fields.

Experimental Section

Materials: Paraformaldehyde (PFA), glutaraldehyde (GA), Triton X-100, ([2-(methacryloyloxy)ethyl] trimethylammonium chloride (METAC), ammonium persulfate (APS), N,N,N′,N′-tetramethylethylenediamine (TEMED), ammonium tetrachloropalladate(II) ($(NH_4)_2PdCl_4$), formaldehyde (HCHO), gold(III) chloride trihydrate ($HAuCl_4 \cdot 3H_2O$), 1,3,6,8-pyrenetetrasulfonic acid tetrasodium salt (4-PSA), 1,1′-dioctadecyl-3,3,3′,3′-tetramethylindocarbocyanine perchlorate (Dil), hexamethyldisilazane (HMDS), polymethyl methacrylate (PMMA, 120k), methyl methacrylate (MMA), and polyethylene glycol (PEG, Mw 300) were purchased from Sigma-Aldrich. Acrylic acid N-hydroxysuccinimide ester (NHS-AA), dimethylamine borane (DMAB), ethylenediaminetetraacetic acid (EDTA), and boracic acid (H_3BO_3) were purchased from J&K Scientific Ltd. Copper(II) sulfate pentahydrate ($CuSO_4 \cdot 5H_2O$), copper(II) chloride dihydrate ($CuCl_2$), nickel(II) sulfate hexahydrate ($NiSO_4 \cdot 6H_2O$), silver nitrate ($AgNO_3$) were purchased from UNI-CHEM. Potassium sodium tartrate tetrahydrate ($KNaC_4H_4O_6 \cdot 4H_2O$), sodium hypophosphite monohydrate ($NaH_2PO_2 \cdot H_2O$), sodium acetate (CH_3COONa), sodium hydrogen carbonate ($NaHCO_3$), and sodium hydroxide (NaOH) were purchased from VWR chemicals. Lactic acid, trisodium citrate were purchased from Acros organics. Ammonia solution ($NH_3 \cdot H_2O$) was purchased from International Laboratory USA. METAC was precipitated in acetone and washed several times with acetone before use. C2C12, HeLa, and HCT8 cells were cultured in cell culture medium (Dulbecco's modified Eagle medium (DMEM) for C2C12, RPMI 1640 for HeLa and HCT8 cells) supplemented with 10% fetal bovine serum (FBS), 1% penicillin-streptomycin at 37 °C and 5% CO_2, and were passaged at approximately 90% confluency. The reagents used for cell culture including DMEM, RPMI 1640, FBS, penicillin streptomycin, trypsin, and phosphate buffered saline (PBS) were purchased from Life Technologies.

Process of polymer-assisted cell metallization: C2C12 cells adhered on clean glass slides for 20 min were fixed with fixation agent (3% PFA and 0.1% GA) for 15 min at room temperature (R.T.). The fixed cells were treated with Triton X-100 (0.2% in PBS, 10 min, R.T.) to enhance the permeability of cell membrane. Then, the pretreated cells were washed with PBS for 3 times and incubated with NHS-AA (20 mM in PBS) for 2 h at R.T. to modify the cells with vinyl group. After modification and washing with PBS for 3 times, the modified cells were perfused with freshly prepared polymerization reagents (7.5% METAC, 0.2% APS, and 0.2% TEMED) for 5 min at 4 ℃, followed by performing the polymerization at 37 ℃ water bath for different durations. After polymerization and washing with deionized (DI) water 3 times, the cells were incubated into a 5 mM $(NH_4)_2PdCl_4$ aqueous solution for 15 min in a dark environment to allow ion exchange. After ion exchange, the cells were washed 5 times by DI water and immersed in water overnight to remove the nonspecifically adsorbed $PdCl_4^{2-}$ ions. After washing, the cells were metallized by different metals according to the following procedures.

Metallization of Cu: Metallization of Cu was carried out in two steps. In step one, a Cu-HCHO solution consisting of a 1:1 (v/v) mixture of solution A (NaOH (12 g L^{-1}), $CuSO_4 \cdot 5H_2O$ (13 g L^{-1}), and $KNaC_4H_4O_6 \cdot 4H_2O$ (29 g L^{-1}) in DI water) and solution B (HCHO, 9.5 mL L^{-1} in DI water) was used. The samples were immersed in the Cu-HCHO bath for 5 min to metallize the cell surface. To sufficiently metallize the interior of the cells, a second step of metallization was needed using a Cu-DMAB solution for 20 min.[51] The Cu-DMAB solution consisted of $CuCl_2$ (50 mM), EDTA (50 mM), H_3BO_3 (100 mM), and DMAB (100 mM) in aqueous. The pH was adjusted to 7.0 with 1 M NaOH.

Metallization of Ni: The metallization of Ni was carried out at 37 ℃ for 30 min in an aqueous solution containing $NiSO_4 \cdot 6H_2O$ (25 g L^{-1}), CH_3COONa (20 g L^{-1}), $NaHCO_3$ (12 g L^{-1}), lactic acid (21 mL L^{-1}) and $NaH_2PO_2 \cdot H_2O$ (20 g L^{-1}). For fabrication of magnetic C2C12-Ni

biocomposites, the suspended C2C12 cells after polymerization and $PdCl_4^{2-}$ loading were metallized at R.T. for 5 min in Ni plating bath contains $NiSO_4 \cdot 6H_2O$ (40 g L^{-1}), trisodium citrate (20 g L^{-1}), lactic acid (10 g L^{-1}) and DMAB (1 g L^{-1}) with pH 7.5 adjusted by $NH_3 \cdot H_2O$.

Metallization of Ag: The metallization of HCT8 cells was conducted at R.T. in an aqueous $Ag(NH_3)_2^+$ solution using glucose as reductant. The $Ag(NH_3)_2^+$ solution contained $AgNO_3$ (30 g L^{-1}), $NH_3 \cdot H_2O$ (200 mL L^{-1}) and NaOH (0.6 M). The reductant solution contains $C_6H_{12}O_6$ (45 g L^{-1}), $KNaC_4H_6O_6$ (5 g L^{-1}), and alcohol (100 mL L^{-1}) in water. The suspended HCT8 cells (~ 3×10^5 cells) were first added into the reductant solution (10 mL) and then the $Ag(NH_3)_2^+$ solution (2 mL) was dropwise added into the above reductant solution. The Ag metallization process was conducted at R.T. for 20 min.

Bimetallic biocomposites: The galvanic displacement reaction was employed to fabricate Au/Cu bimetallic biocomposites. The suspended HCT8 cells were first metallized by Cu through PACM method. The obtained HCT8-Cu biocomposites were then incubated into 1 mM $HAuCl_4$ in water to carried out galvanic displacement reaction. After galvanic displacement for 5 min, the Au/Cu bimetallic cells with original morphologies can be obtained.

Fluorescent study: Negatively charged fluorescent probe 1,3,6,8-pyrenetetrasulfonic acid tetrasodium salt (4-PSA) was exploited to indicate the polymer chains. Cells adhered on glass (after polymerization) were washed 3 times with DI water and then incubated with 4-PSA (1 mM in PBS) overnight. The cell samples were then washed again 5 times to remove the loosely attached fluorescent dyes. To indicate the cell profile, cell membrane was stained by Dil (1 μM) for 10 min before polymerization. The cell samples were then observed under confocal microscope (Leica TCS SPE).

Determination of $PdCl_4^{2-}$ after ion exchange: The immobilization of $PdCl_4^{2-}$ was characterized by inductively coupled plasma optical emission spectrometer (ICP-OES) as follows. 1.5×10^5 C2C12 cells were firstly seeded in a 12-well plate, followed by the polymerization and ion exchange steps. After thorough wash with DI water, the samples were incubated in 0.5 mL aqua regia (HNO_3:HCl = 1:3) for 20 min under sonication, followed by adding 9.5 mL distilled water. The amount of Pd elements in different cell samples was analyzed by ICP-OES (Agilent Technologies 5100).

Cell dehydration and characterization: For SEM characterization of non-metallized cells, the cells were fixed and dehydrated as follows. First, the cells were fixed with fixation agent (3% PFA and 0.1% GA) for 15 min at room temperature (R.T.). Then, the cells were dehydrated by using sequential washes with ethanol (30%, 50%, 70%, 80%, 95%, 100%, and 100%, 15 min each) and HMDS (50% in ethanol, 100%, and 100%, 15 min each) at room temperature. Finally, dehydrated cell samples were sputtered with gold for scanning electron microscope observation (FESEM, JSM6335F, JEOL, Japan). For dehydration of metallized cells, cell samples after metallization were washed by water and dehydrated by using 15-min long sequential washes in 50% ethanol and 100% ethanol and allow to dry in vacuum oven. The morphologies, structures, and elements of the metallized cells were characterized by using scanning electron microscope (SEM, TESCAN VEGA3).

Mechanical measurements: Cells without metallization were probed by AFM. AFM measurements were performed underwater using an Asylum MFP-3D Infinity system (Asylum Research, Oxford Instruments) at RT. Prior to measurement, the sensitivity and spring constant of AFM cantilevers were determined underwater by thermal tuning method. A silicon nitride cantilever with experimentally determined spring constants of 0.047 N m^{-1} and a tip radius of 10 nm was used for mechanical measurements of cells. For collecting force versus indentation

data, the cantilever was first positioned visually above the cell. Then, force curves were recorded at 1 Hz loading rates with a maximum loading force of 5 nN. The elastic modulus is determined by fitting force curves with the Hertz model using Asylum Research software. The Poisson ratio of both cells and cell/metal composites was taken to be 0.5. The mechanical measurements of cells at the early stage of Cu metallization (5 min) and after fully metallization (25 min) were performed by a Hystron-TI 980 Triboindenter system equipped with a Berkovich indenter (Bruker). The loading force was set to 300 μN, and the loading time, holding time, and unloading time were 5 s, 2 s, and 5 s, respectively.

Conductivity and magnetism test: To record the *I-V* curves of single metallic biocomposites, an AFM platform and a Keithley sourcemeter were employed. The C2C12-Cu particles were firstly deposited onto a gold-coated silicon. Then a conductive cantilever probe on AFM was manipulated to approach to the C2C12-Cu particles. After the probe contacted with metallic biocomposites, the current and voltage between the probe and substrate were recorded. Non-metallized cells were also tested as control. The sheet resistance of the C2C12-Cu electrode was tested by a four-point probe method. For magnetic characterization, Lake Shore's fully integrated vibrating sample magnetometer was used to record the magnetization curve of the magnetic C2C12-Ni biocomposites.

Preparation of Wrinkled HCT8-Cu biocomposites: HCT8 cells were digested by trypsin and suspended in DMEM culture medium for 15 min. Then, the macromolecule PEG (75 g L^{-1}, Mw 300) was added into the DMEM solution making the solution hypertonic. The cells were further incubated in the hypertonic solution for 30 min. During incubation, the water inside of cells was released, leading to cell shrink. After incubation, the shrunk cells were fixed and metallized by conducting PACM process.

Preparation of jellyfish-like metallic biocomposites: A layer of PMMA was used as sacrificial layer. C2C12 cells were first adhered onto PMMA-coated glass substrates for 20 min. Then the adhered cells were metallized with Cu by PACM method only in the Cu-HCHO plating solution for 5 min. Then, the PMMA layer was dissolved by using acetone, producing the suspended hollow metallic cells. To prepare the bubble-propelled micromotors, Pt was deposited into the cavity of the jellyfish-like biocomposites. To deposit Pt, the C2C12 cells were first metallized in Cu-HCHO plating solution for 1 min and then incubated into 2 mM H_2PtCl_6 solution for 1.5 min to carry out the displacement reaction. Next, the Pt-decorated metallic biocomposites were further metallized by Cu for 3 min to form a surface layer. Lastly, the jellyfish-like microrobots were collected by dissolving the PMMA sacrificial layer.

Electrochemical measurements of HER on electrodes: The electrochemical measurements were carried out at room temperature in a three-electrode glass cell connected to an electrochemical workstation (CHI 660E). Linear sweep voltammetry with a scan rate of 5 $mV \cdot s^{-1}$ was carried out in 0.5 M H_2SO_4 solution by using a saturated calomel electrode as the reference electrode and a Pt plate as the counter electrode. The hydrogen bubble production and detachment behavior were recorded by applying overpotentials of 0.6 V and 0.8 V for the C2C12-Cu electrode and the flat Cu electrode, respectively. The flat Cu electrode was prepared by thermal evaporation deposition of Cu on PET. The electrodes with similar sheet resistance ($R \approx 0.28\ \Omega\ sq^{-1}$) were used for electrochemical measurements.

Manipulation of living cells with magnetic biocomposites: Biohybrids assembled by C2C12-Ni biocomposites and living C2C12 cells were used to manipulate living cells. Prior to prepare the assembled biohybrid, C2C12-Ni biocomposites were first coated with a layer of Au and then immersed in FBS-containing cell culture medium at 37 ℃ for 1 h. After that, the pretreated C2C12-Ni biocomposites were incubated with living C2C12 cells for 30 min to form stable

biohybrids. The formed biohybrids were extracted from the culture medium under magnetic field and added into a petri dish, on which living cells were preloaded. Then, a magnetism was applied to drive the motion of the biohybrid to push a target cell. The motion of the assembly was observed and recorded under optical microscope (Nikon Eclipse Ni). To quantify the adhesion of metallic biocomposites and smooth polystyrene (PS) microparticles with different cells, C2C12 cells and HCT8 cells (cultured on 1×1 cm^2 PET substrates, with or without fixation) were incubated with the same amount of metallic biocomposites or PS microparticles (5×10^5 particles mL^{-1}, 200 μL, respectively) for 15 min, followed by washing with PBS and counting under microscopy.

Supporting Information
Supporting Information is available from the Wiley Online Library or from the author.

Acknowledgements
We acknowledge the financial support from University Grant Council through NSFC/RGC Joint Research Scheme (N_PolyU528/16), National Natural Science Foundation of China (22035008).

Received: ((will be filled in by the editorial staff))
Revised: ((will be filled in by the editorial staff))
Published online: ((will be filled in by the editorial staff))

References

[1] S. Sotiropoulou, Y. Sierra-Sastre, S. S. Mark, C. A. Batt, *Chem. Mater.* **2008**, *20*, 821.

[2] X. Li, Y. Li, J. Cai, D. Zhang, *Sci. China Ser. E* **2003**, *46*, 161.

[3] C. Mao, D. J. Solis, B. D. Reiss, S. T. Kottmann, R. Y. Sweeney, A. Hayhurst, G. Georgiou, B. Iverson, A. M. Belcher, *Science* **2004**, *303*, 213.

[4] Y. Lee, J. Kim, D. S. Yun, Y. S. Nam, Y. Shao-Horn, A. M. Belcher, *Energ. Environ. Sci.* **2012**, *5*, 8328.

[5] J. F. Ohmura, F. J. Burpo, C. J. Lescott, A. Ransil, Y. Yoon, W. C. Records, A. M. Belcher, *Nanoscale* **2019**, *11*, 1091.

[6] Y. Huang, C. Y. Chiang, S. K. Lee, Y. Gao, E. L. Hu, J. De Yoreo, A. M. Belcher, *Nano Lett.* **2005**, *5*, 1429.

[7] K. T. Nam, D. W. Kim, P. J. Yoo, C. Y. Chiang, N. Meethong, P. T. Hammond, Y. M. Chiang, A. M. Belcher, *Science* **2006**, *312*, 885.

[8] Y. J. Lee, Y. Lee, D. Oh, T. Chen, G. Ceder, A. M. Belcher, *Nano Lett.* **2010**, *10*, 2433.

[9] D. Oh, J. Qi, Y.-C. Lu, Y. Zhang, Y. Shao-Horn, A. M. Belcher, *Nat. Commun.* **2013**, *4*, 2756.

[10] X. Li, J. Cai, Y. Shi, Y. Yue, D. Zhang, *ACS Appl. Mater. Interfaces* **2017**, *9*, 1593.

[11] L. Sun, D. Zhang, Y. Sun, S. Wang, J. Cai, *Adv. Funct. Mater.* **2018**, *28*, 1707231.

[12] M. Knez, A. M. Bittner, F. Boes, C. Wege, H. Jeske, E. Maiβ, K. Kern, *Nano Lett.* **2003**, *3*, 1079.

[13] Z. Deng, C. Mao, *Nano Lett.* **2003**, *3*, 1545.

[14] W. E. Ford, O. Harnack, A. Yasuda, J. M. Wessels, *Adv. Mater.* ***2001***, 13, 1793.

[15] L. Wu, W. Wang, W. Zhang, H. Su, Q. Liu, J. Gu, T. Deng, D. Zhang, *NPG Asia Mater.* **2018**, *10*, e462.

[16] G. Karp, *Cell and Molecular Biology: Concepts and Experiments*, John Wiley & Sons, **2009**.

[17] B. Kaehr, J. L. Townson, R. M. Kalinich, Y. H. Awad, B. S. Swartzentruber, D. R. Dunphy, C. J. Brinker, *Proc. Natl. Acad. Sci. USA* **2012**, *109*, 17336.

[18] K. C. Meyer, E. N. Coker, D. S. Bolintineanu, B. Kaehr, *J. Am. Chem. Soc.* **2014**, *136*, 13138.

[19] C. Huang, G. Yang, Q. Ha, J. Meng, S. Wang, *Adv. Mater.* **2015**, *27*, 310.

[20] W. Wang, H. Cui, P. Zhang, J. Meng, F. Zhang, S. Wang, *ACS Appl. Mater. Interfaces* **2017**, *9*, 10537.

[21] W. Zhu, J. Guo, S. Amini, Y. Ju, J. O. Agola, A. Zimpel, J. Shang, A. Noureddine, F. Caruso, S. Wuttke, J. G. Croissant, C. J. Brinker, *Adv. Mater.* **2019**, *31*, 1900545.

[22] K. C. Meyer, N. R. Labriola, E. M. Darling, B. Kaehr, *Adv. Biosyst.* **2019**, *3*, 1800285.

[23] J. L. Townson, Y. S. Lin, S. S. Chou, Y. H. Awad, E. N. Coker, C. J. Brinker, B. Kaehr, *Nat. Commun.* **2014**, *5*, 5665.

[24] F. Caruso, E. Donath, H. Mohwald, R. Georgieva, *Macromolecules* **1998**, *31*, 7365.

[25] A. S. Angelatos, Y. Wang, F. Caruso, *Langmuir* **2008**, *24*, 4224.

[26] E. Rettler, S. Hoeppener, B. W. Sigusch, U. S. Schubert, *J. Mater. Chem. B* **2013**, *1*, 2789.

[27] X. Xia, Y. Wang, A. Ruditskiy, Y. Xia, *Adv. Mater.* **2013**, *25*, 6313.

[28] L. M. Moreau, C. A. Schurman, S. Kewalramani, M. M. Shahjamali, C. A. Mirkin, M. J. Bedzyk, *J. Am. Chem. Soc.* **2017**, *139*, 12291.

[29] E. González, J. Arbiol, V. F. Puntes, *Science* **2011**, *334*, 1377.

[30] Z. Lu, W. Zhu, X. Yu, H. Zhang, Y. Li, X. Sun, X. Wang, H. Wang, J. Wang, J. Luo, X. Lei, L. Jiang, *Adv. Mater.* **2014**, *26*, 2683.

[31] Z. Lu, M. Sun, T. Xu, Y. Li, W. Xu, Z. Chang, Y. Ding, X. Sun, L. Jiang, *Adv. Mater.* **2015**, *27*, 2361.

[32] P. Wang, T. Hayashi, Q. Meng, Q. Wang, H. Liu, K. Hashimoto, L. Jiang, *Small* **2017**, *13*, 1601250.

[33] W. Xu, Z. Lu, X. Sun, L. Jiang, X. Duan, *Acc. Chem. Res.* **2018**, *51*, 1590.

[34] H. Li, S. Chen, Y. Zhang, Q. Zhang, X. Jia, Q. Zhang, L. Gu, X. Sun, L. Song, X. Wang, *Nat. Commun.* **2018**, *9*, 2452.

[35] D. Wakerley, S. Lamaison, F. Ozanam, N. Menguy, D. Mercier, P. Marcus, M. Fontecave, V. Mougel, *Nat. Mater.* **2019**, *18*, 1222.

[36] S. H. Yang, K. B. Lee, B. Kong, J. H. Kim, H. S. Kim, I. S. Choi, *Angew. Chem. Int. Ed.* **2009**, *48*, 9160.

[37] J. Lee, J. Choi, J. H. Park, M. H. Kim, D. Hong, H. Cho, S. H. Yang, I. S. Choi, *Angew. Chem. Int. Ed.* **2014**, *53*, 8056.

[38] J. H. Park, D. Hong, J. Lee, I. S. Choi, *Acc. Chem. Res.* **2016**, *49*, 792.

[39] W. Youn, J. Y. Kim, J. Park, N. Kim, H. Choi, H. Cho, I. S. Choi, *Adv. Mater.* **2020**, *32*, 1907001.

[40] J. Niu, D. J. Lunn, A. Pusuluri, J. I. Yoo, M. A. O'Malley, S. Mitragotri, H. T. Soh, C. J. Hawker, *Nat. Chem.* **2017**, *9*, 537.

[41] Y. Zhao, M. Fan, Y. Chen, Z. Liu, C. Shao, B. Jin, X. Wang, L. Hui, S. Wang, Z. Liao, D. Ling, R. Tang, B. Wang, *Sci. Adv.* **2020**, *6*, eaaw9679.

[42] J. Geng, W. Li, Y. Zhang, N. Thottappillil, J. Clavadetscher, A. Lilienkampf, M. Bradley, *Nat. Chem.* **2019**, *11*, 578.

[43] F. Chen, P. W. Tillberg, E. S. Boyden, *Science* **2015**, *347*, 543.

[44] J. R. Moffitt, J. Hao, D. Bambah-Mukku, T. Lu, C. Dulac, X. Zhuang, *Proc. Natl. Acad. Sci. USA* **2016**, *113*, 14456.

[45] J. Liu, Y. S. Kim, C. E. Richardson, A. Tom, C. Ramakrishnan, F. Birey, T. Katsumata, S. Chen, C. Wang, X. Wang, L. M. Joubert, Y. Jiang, H. Wang, L. E. Fenno, J. B. H. Tok, S. P. Pasca, K. Shen, Z. Bao, K. Deisseroth, *Science* **2020**, *367*, 1372.

[46] Y. Yu, C. Yan, Z. Zheng, *Adv. Mater.* **2014**, *26*, 5508.

[47] X. Wang, H. Hu, Y. Shen, X. Zhou, Z. Zheng, *Adv. Mater.* **2011**, *23*, 3090.

[48] Y. Yu, J. Zeng, C. Chen, Z. Xie, R. Guo, Z. Liu, X. Zhou, Y. Yang, Z. Zheng, *Adv. Mater.* **2014**, *26*, 810.

[49] Y. Yu, Y. Yu, X. Xiao, Y. Zhang, K. Li, C. Yan, X. Wei, L. Chen, H. Zhen, H. Zhou, S. Zhang, Z. Zheng, *Adv. Mater.* **2016**, *28*, 4926.

[50] P. Li, Y. Zhang, Z. Zheng, *Adv. Mater.* **2019**, *31*, 1902987.

[51] H. Lee, S. M. Dellatore, W. M. Miller, P. B. Messersmith, *Science* **2017**, *318*, 426.

Figures

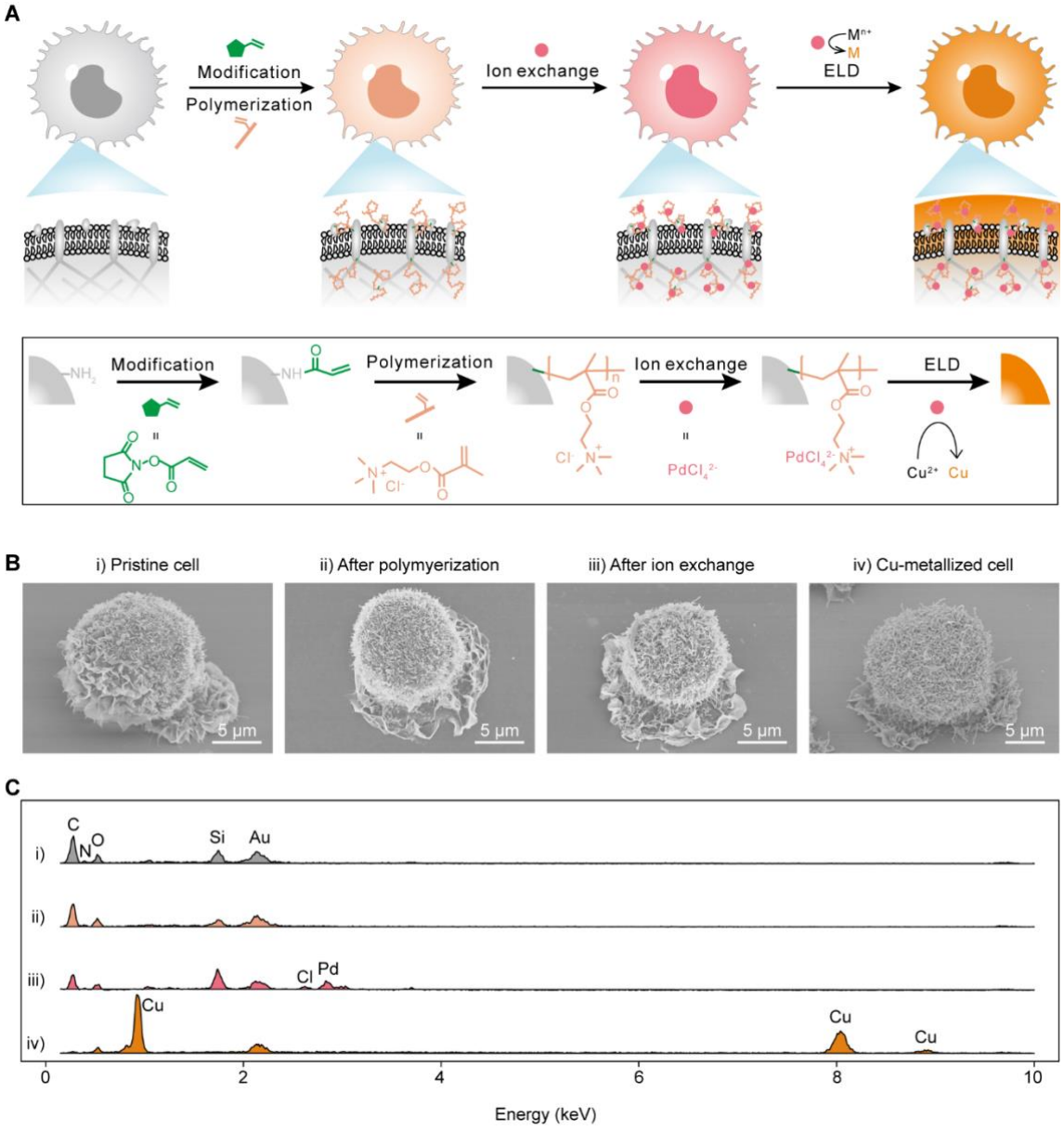

Figure 1. Schematic illustration of polymer-assisted cell metallization (PACM) for the preparation of metallic biocomposites using mammalian cells as templates. A) The PACM procedure. B) Cell morphology at different PACM steps. C) The energy dispersive spectroscopy spectra of cells at different PACM stages: (i) the pristine cells; (ii) the cells after polymerization of METAC; (iii) the cells after adsorption of $PdCl_4^{2-}$; (iv) the Cu-metallized cells. The signals of Si and Au elements were generated by the glass substrate and the sputtered gold film, respectively.

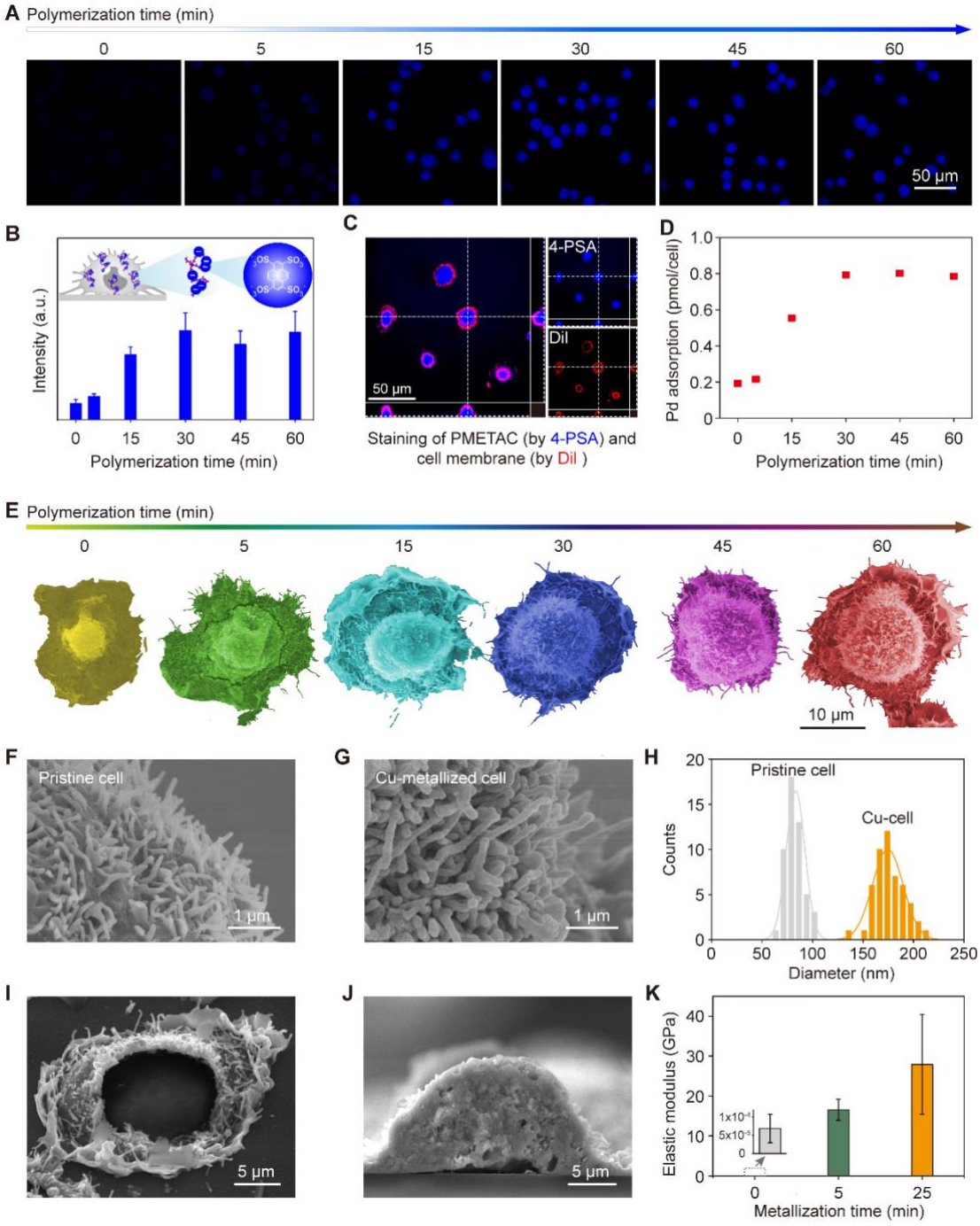

Figure 2. Evaluation of grafted polymer chains and their effect on cell metallization. A) Fluorescent image of negatively charged 4-PSA dyes adsorbed by cells with different polymerization durations. B) Schematic illustration of cells stained by 4-PSA dyes and the fluorescence intensity of anchored 4-PSA with extended polymerization time. C) The confocal fluorescent images of stained cells. The cell membrane was stained by DiI, and the produced polymer chains were indicated by 4-PSA. The co-location of DiI and 4-PSA on cell membrane

demonstrated the cell surface grafting of polymer chains. Meanwhile, the intracellular 4-PSA signal confirmed the polymerization inside of cells. D) The determination of anchored Pd in cells with extended polymerization time. E) The morphological evolution of cells with different polymerization time after metallization by Cu. F,G) The surface villi structures of a pristine (F) and a Cu-metallized (G) C2C12 cell. H) Comparison of the diameter of villi structures on pristine cells and on Cu metallized cells. I,J) The cell surface metallization and intracellular metallization at the early stage (5 min) (I) and at the later stage (25 min) (J) of Cu metallization. K) The elastic modulus of cells and cell/metal composites metallized with different durations.

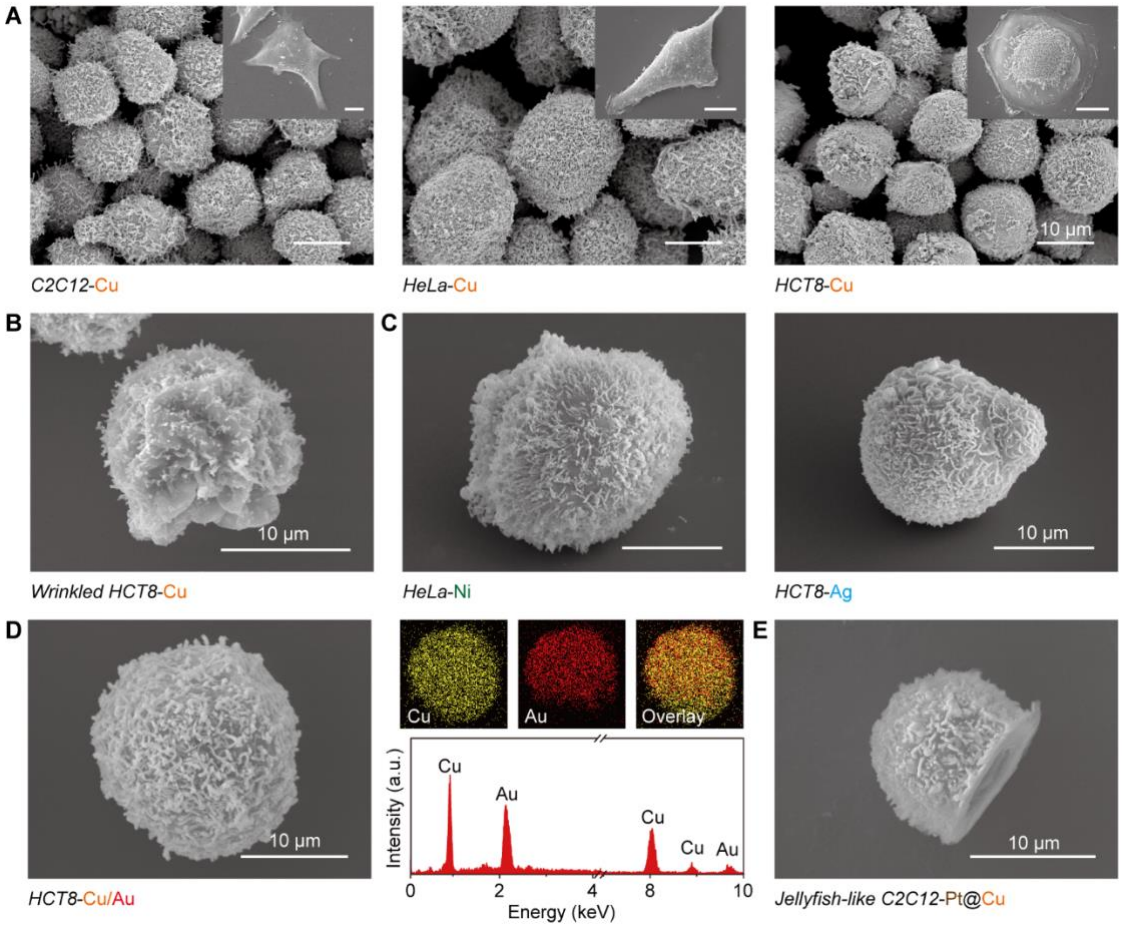

Figure 3. The generality and versatility of the PACM method. A) PACM using different cell templates including C2C12 cells, HeLa cells, and HCT8 cells. Insert shows the spread cells after Cu metallization. B) Morphology of a wrinkled metallic biocomposite. C) Metallization of Ni and Ag using HeLa cells and HCT8 cells as templates, respectively. D) Morphology and element analysis of Cu/Au bimetallic biocomposites. E) Morphology of jellyfish-like Janus biocomposites.

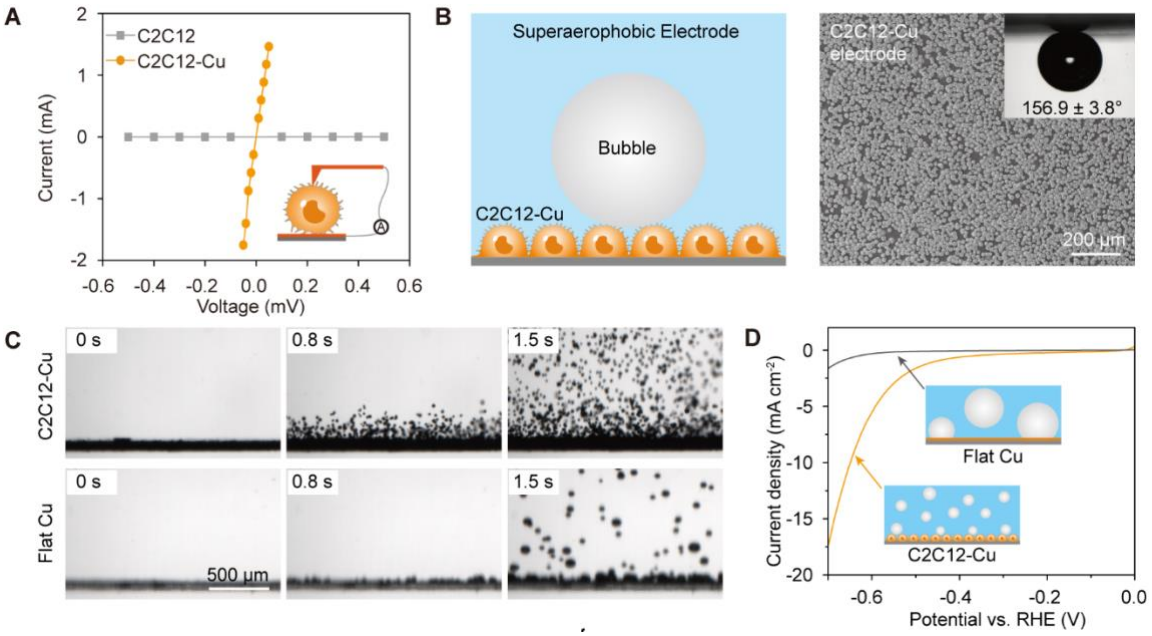

Figure 4. Construction of the cell-templated superaerophobic electrode for hydrogen evolution reaction (HER). A) Conductivity test of single C2C12-Cu metallic biocomposites. A conductive probe mounted on AFM platform was employed to contact and record the *I-V* curve of single metallic biocomposites. B) Schematic illustration and SEM image of the C2C12-Cu electrode with superaerphobic property. Insert shows the underwater gas bubble contact angle of the electrode. C) Digital images of bubble generation and detachment behavior on the C2C12-Cu electrode and the flat Cu electrode during HER. D) Polarization curves of the C2C12-Cu electrode and the flat Cu electrode for HER, showing that the superaerophobic C2C12-Cu electrode affords much faster current promotion.

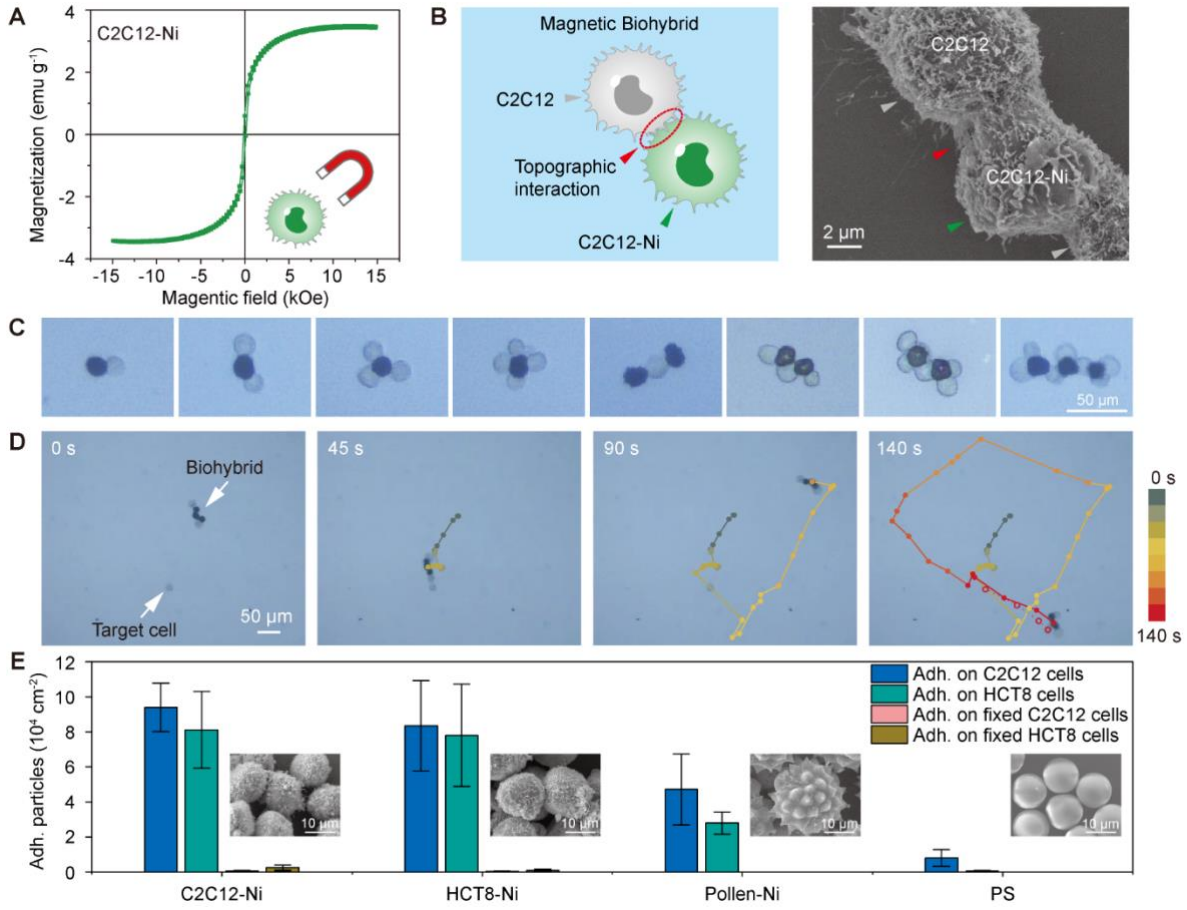

Figure 5. Construction of stable magnetic biohybrids for cell manipulation. A) Magnetization curve of C2C12-Ni metallic biocomposites. B) Formation of magnetic biohybrids through topographic interaction between living cells and cell-templated metallic biocomposites. C) Magnetic biohybrids assembled by living C2C12 cells and C2C12-Ni biocomposites with different formats. D) Manipulation of living cells by using magnetic C2C12-Ni biocomposites. The arrows in the left image indicate a target cell and a magnetic biohybrid. The biohybrid was used to manipulate living cells under a magnetic field. The solid line and the dot line show the trajectory of the biohybrid and the target living cell, respectively. E) Adhesion of cell-templated magnetic microparticles (C2C12-Ni and HCT8-Ni), metallic chrysanthemum pollen grains (pollen-Ni), and smooth polystyrene (PS) microparticles on living and fixed cells (C2C12 cells and HCT8 cells). Inserts show the morphology of the C2C12-Ni, HCT8-Ni, pollen-Ni, and the PS microparticles.

Transformation of mammalian cells into metallic biocomposites with good preservation of original cellular structures and metallic properties is achieved by taking advantage of polymer chains grafted on and within the cells. The polymer-assisted cell metallization (PACM) is a versatile biotemplating strategy to fabricate functional metallic biocomposites with different cell types, architectures, and compositions of metal.

W. Wang, Q. Gan, Y. Zhang, X. Lu, H. Wang, Y. Zhang, H. Hu, L. Chen, L. Shi, S. Wang, Z. Zheng*

Polymer-assisted metallization of mammalian cells

ToC figure

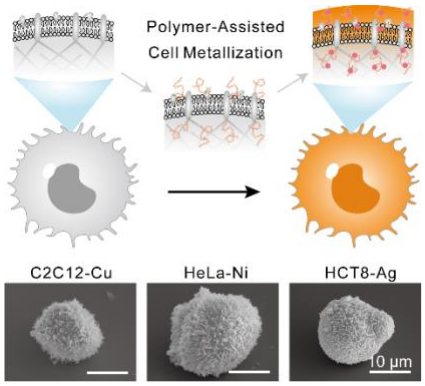

Supporting Information

Polymer-assisted metallization of mammalian cells

*Wenshuo Wang, Qi Gan, Yuqi Zhang, Xi Lu, Huixin Wang, Yaokang Zhang, Hong Hu, Lina Chen, Lianxin Shi, Shutao Wang, Zijian Zheng**

Dr. W. Wang, Dr. Q. Gan, Dr. Y. Zhang, Dr. X. Lu, H. Wang, Dr. Y. Zhang, Dr. H. Hu, Dr. L. Chen, Prof. Z. Zheng
Laboratory for Advanced Interfacial Materials and Devices,
Institute of Textiles and Clothing,
The Hong Kong Polytechnic University,
Hong Kong SAR, China
E-mail: tczzheng@polyu.edu.hk

Dr. L. Shi, Prof. S. Wang
CAS Key Laboratory of Bio-inspired Materials and Interfacial Science,
CAS Center for Excellence in Nanoscience,
Technical Institute of Physics and Chemistry, Chinese Academy of Sciences,
Beijing, 100190, P. R. China

Prof. S. Wang
School of Future Technology,
University of Chinese Academy of Sciences,
Beijing, 100049, P. R. China

Keywords: cell metallization, polymer-assisted metal deposition, biotemplating, biocomposites, nanomaterials

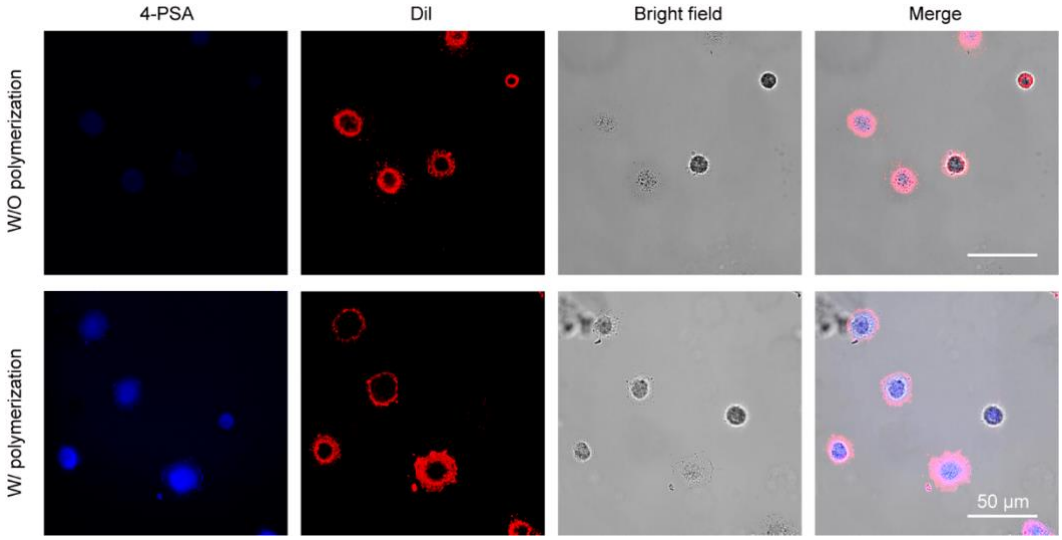

Figure S1. Fluorescent characterization of adsorbed 4-PSA dyes in cells without and with the polymerization step. The fluorescent signal of 4-PSA (blue) in cells without polymerization was very weak, while the cells with polymerization showed strong fluorescent signal. The dye Dil (red) was used for cell membrane staining.

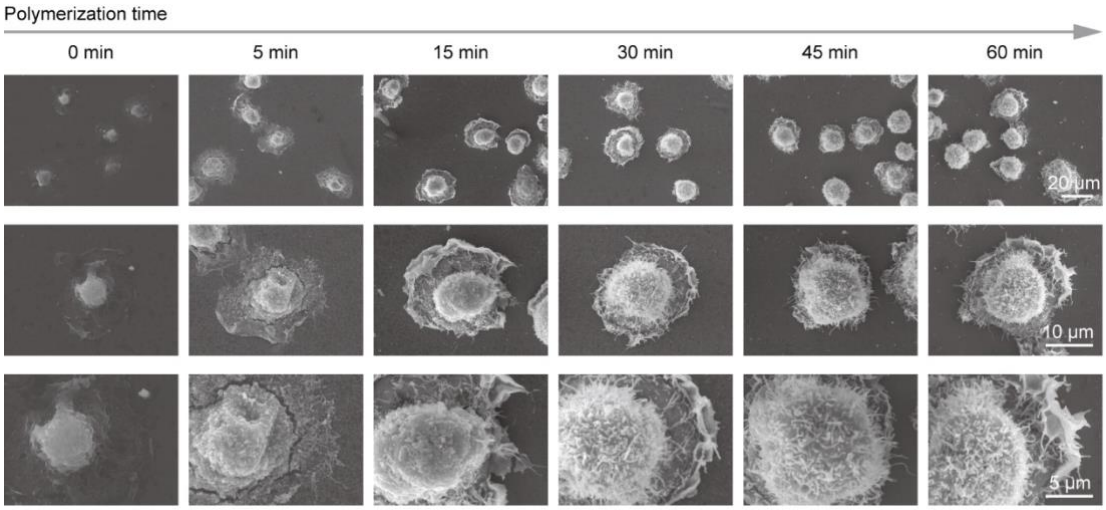

Figure S2. Morphological characterization of Cu-metallized C2C12 cells with different polymerization time. The SEM images zoomed in from top to bottom.

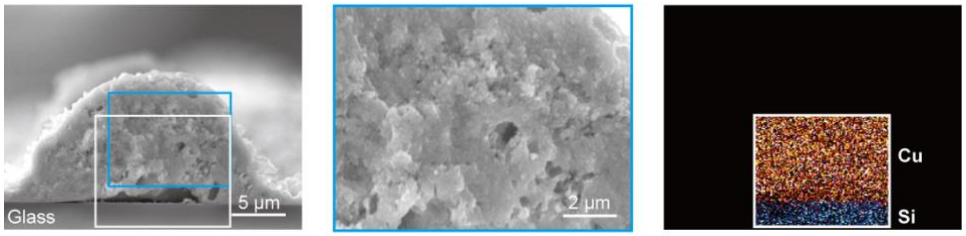

Figure S3. Characterization of intracellular metallization. Cross-sectional SEM image and EDS mapping indicated the deposition of Cu inside of C2C12 cells via PACM.

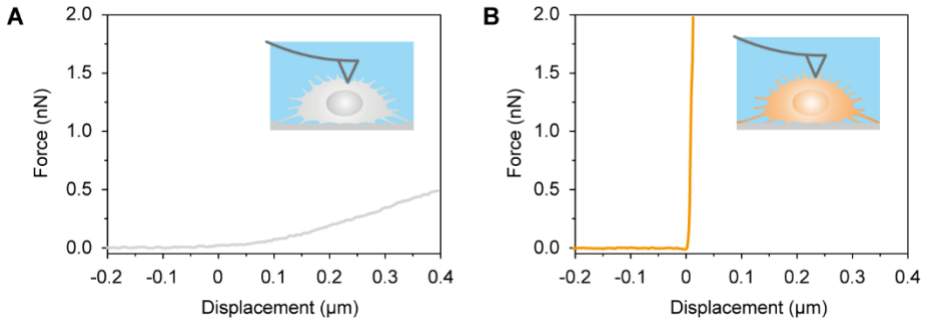

Figure S4. Mechanical characterization of cells by AFM. A) The AFM-derived force-displacement curve of C2C12 cells before Cu metallization. B) The force-displacement curve of C2C12 cell after Cu metallization.

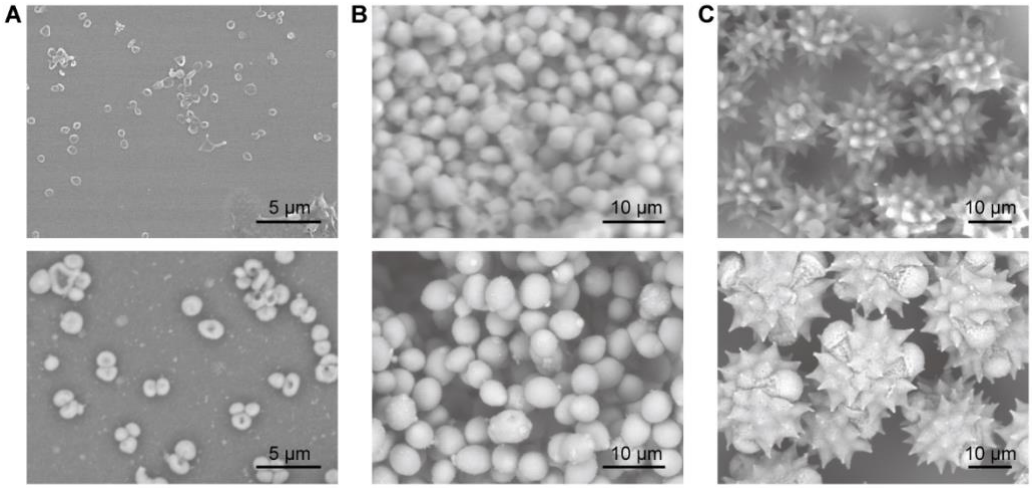

Figure S5. Polymer-assisted metallization of other biological templates. A-C) Morphological characterization of (A) extracellular vesicles excreted from HCT8 cells, (B) yeast, and (C) chrysanthemum pollen grains before (top) and after (bottom) Cu metallization via polymer-assisted metallization strategy.

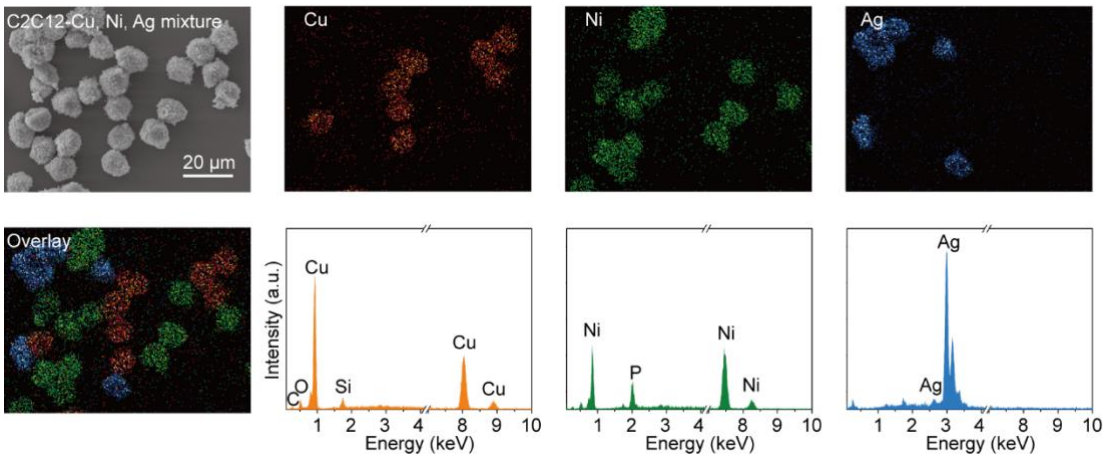

Figure S6. Elemental analysis of metallic biocomposites templated from C2C12 cells. The Cu-, Ni-, and Ag-metallized C2C12 cells were mixed and then characterized under SEM.

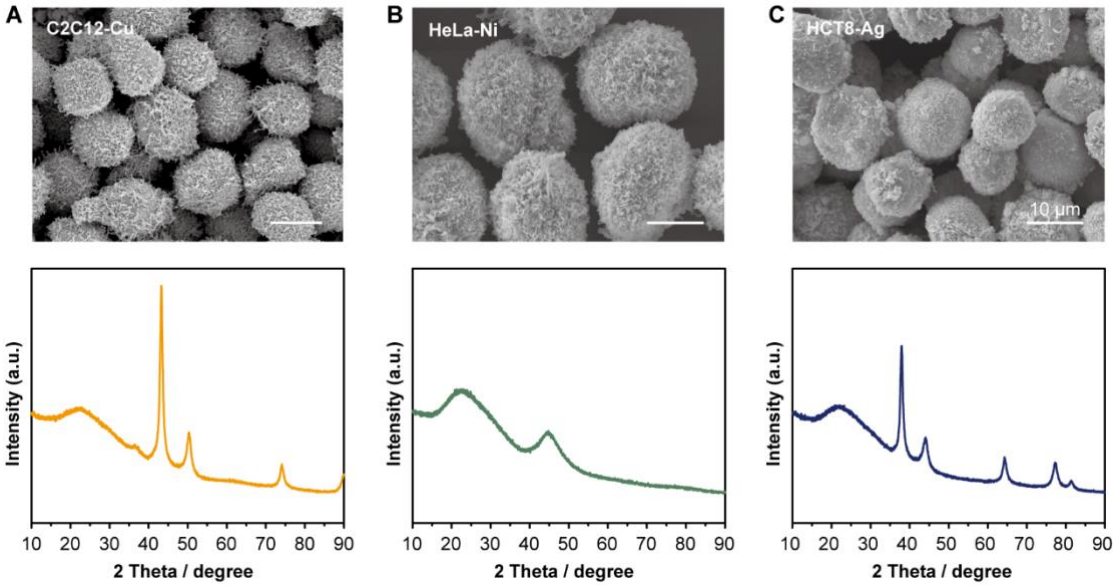

Figure S7. SEM and XRD characterizations of different metallic biocomposites. A) C2C12 cells metallized by Cu. B) HeLa cells metallized by Ni. C) HCT8 cells metallized by Ag.

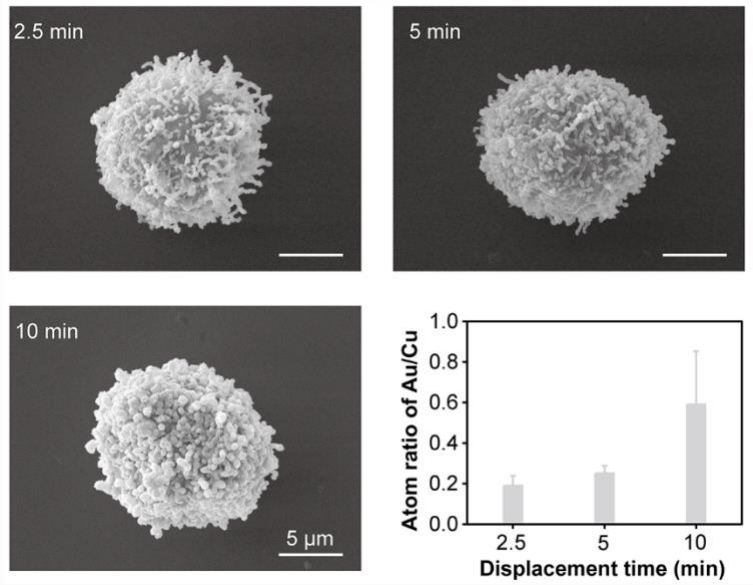

Figure S8. Morphological and atomic evolution of Cu/Au bimetallic biocomposites with increased displacement reaction time. The galvanic displacement reaction was conducted for different durations from 2.5 min to 10 min.

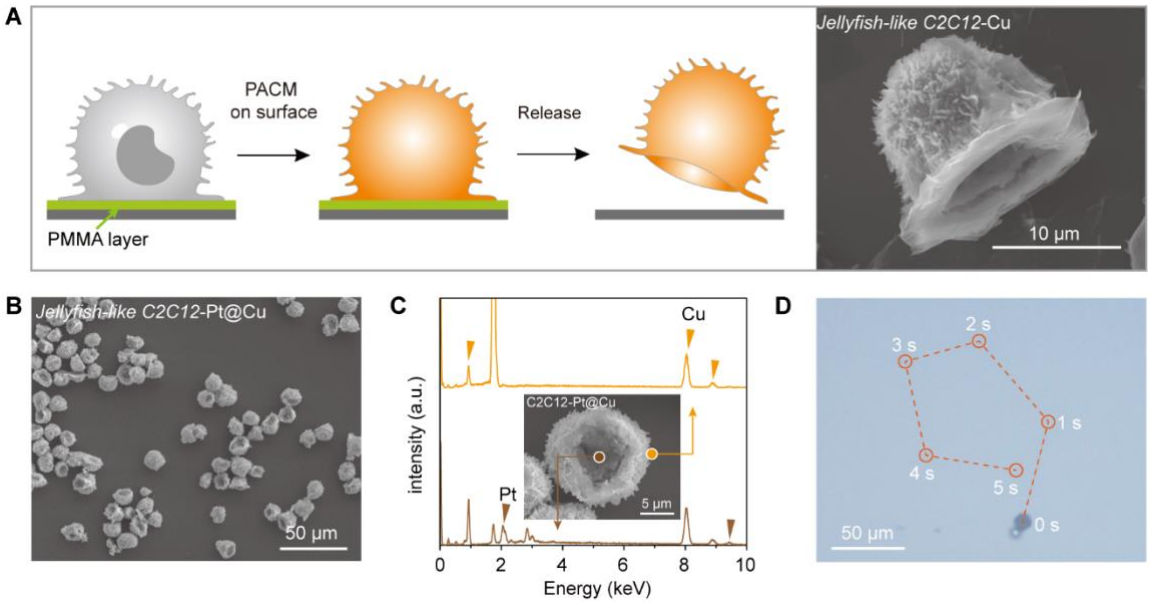

Figure S9. Fabrication of jellyfish-like metallic biocomposites. A) Fabrication procedure and morphology of jellyfish-like C2C12-Cu biocomposites. B) Morphology of jellyfish-like C2C12-Pt@Cu biocomposites. C) Asymmetric distribution of Pt on the Janus biocomposites. D) Motion trajectory of a Pt-decorated Janus biocomposite in 5% H_2O_2 solution.

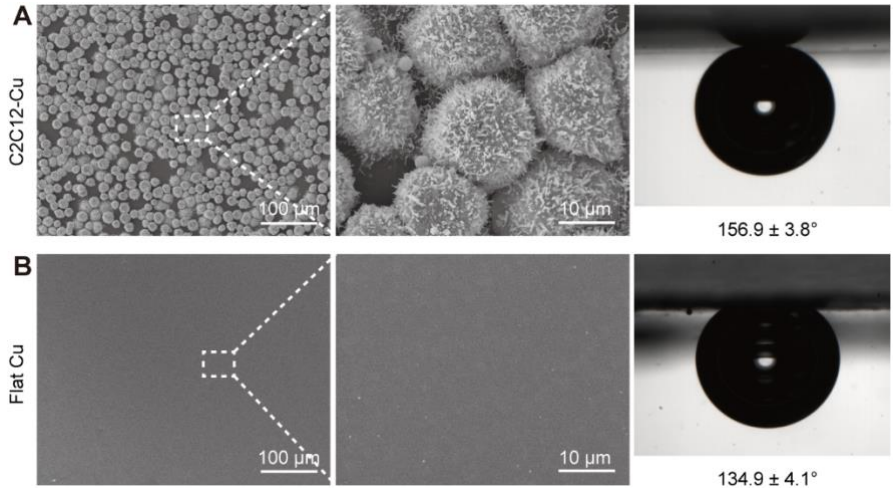

Figure S10. Morphological features and underwater gas bubble contact angles of the C2C12-Cu electrode and the flat Cu electrode. A) SEM images and contact angle of gas bubble showing hierarchical structures and superaerophobic property of the C2C12-Cu electrode. B) SEM images and contact angle of gas bubble showing the flat surface and aerophobic property of the flat Cu electrode.

Movie S1. Movement of a Pt-decorated Janus micromotor in 5% H_2O_2 solution.

Movie S2. Manipulation of living cells by using C2C12-Ni metallic biocomposites.